

# Electron phonon coupling and superconductivity in $\alpha$ -MoB<sub>2</sub> as a function of pressure

M-A Carmona-Galván<sup>1,3</sup>, R Heid<sup>2</sup>, and O De la Peña-Seaman<sup>3</sup>

<sup>1</sup> Facultad de Ciencias Físico Matemáticas (FCFM), Benemérita Universidad Autónoma de Puebla, Apartado Postal 1152 C.P. 72000 Puebla, Puebla, México

<sup>2</sup> Institut für QuantenMaterialien und Technologien, Karlsruher Institut für Technologie (KIT), D-76021 Karlsruhe, Germany

<sup>3</sup> Instituto de Física “Ing. Luis Rivera Terrazas”, Benemérita Universidad Autónoma de Puebla, Av. San Claudio & Blvd. 18 Sur, Ciudad Universitaria, C.P. 72570, Puebla, Puebla, México

E-mail: oseaman@ifuap.buap.mx

**Abstract.** We have studied the lattice dynamics, electron-phonon coupling, and superconducting properties of  $\alpha$ -MoB<sub>2</sub>, as a function of applied pressure, within the framework of density functional perturbation theory using a mixed-basis pseudopotential method. We found that phonon modes located along the A–H, H–L, and L–A high-symmetry paths exhibit large phonon linewidths and contribute significantly to the electron-phonon coupling constant. Although linewidths are particularly large for the highest-frequency optical phonon modes (dominated by B vibrations), their contribution to the electron-phonon coupling constant is marginal. The latter is largely controlled by the acoustic low-frequency modes of predominantly Mo character. It was observed that at a pressure of 90 GPa, where  $\alpha$ -MoB<sub>2</sub> forms, the phonon-mediated pairing falls into the strong-coupling regime, and the estimate for the superconducting critical temperature  $T_c$  agrees well with experimental observations. When further increasing the applied pressure, a reduction of  $T_c$  is predicted, which correlates with a hardening of the acoustic low-frequency phonon modes and a decrease of the electron-phonon coupling parameter.

*Keywords:* first-principles calculations, phonons, electron-phonon coupling, superconductivity

Submitted to: *PHYSSCR*

## 1. Introduction

The discovery of superconductivity in MgB<sub>2</sub> more than twenty 20 years ago [1], with a critical temperature of  $T_c \approx 39$  K, energized the search for new superconducting materials within the family of diborides. Such a quest was pursued almost immediately after its discovery both experimentally and computationally [2]. After several years of research, the conclusion was reached that MgB<sub>2</sub> is already optimized by nature, in the sense that attempts

to improve its superconducting properties by doping [3–6] or pressure [7, 8] always resulted in a reduction of  $T_c$  in comparison with MgB<sub>2</sub>, or even in a non-superconducting material, like the sibling system AlB<sub>2</sub> [9].

Transition-metal diborides constitute an important sub-class in this context. A typical example studied was NbB<sub>2</sub> with a wide range of measured  $T_c$  from 0.62 K to 9 K [10–12]. MoB<sub>2</sub> attracted attention as well. While it is not a superconductor in its pristine form, superconductivity can be induced by substitution of 4% Zr with a  $T_c \approx 6$  K [13]. It was not until 2022 that the discovery of superconductivity in MoB<sub>2</sub> under applied pressure was reported [14]. At an applied pressure of approximately 20 GPa, MoB<sub>2</sub> becomes superconducting with a very low  $T_c$  of less than 2 K. At these pressures, MoB<sub>2</sub> takes a rhombohedral crystal structure (space group  $R\bar{3}m$ ), known also as  $\beta$ -MoB<sub>2</sub>.  $T_c$  rapidly increases as a function of pressure, reaching  $T_c \approx 27$  K at a pressure of  $p_c \approx 70$  GPa, where it gradually transforms into the hexagonal  $\alpha$ -MoB<sub>2</sub> structure (space group  $P6/mmm$ ,  $D_{6h}^1$  no.191 [15]). With further increase of pressure,  $\alpha$ -MoB<sub>2</sub> experiences a less dramatic  $T_c$  increase, which culminates at 110 GPa in a maximum  $T_c$  of 32.4 K [14].

Theoretical calculations have suggested that the mechanism for such a high  $T_c$  value in  $\alpha$ -MoB<sub>2</sub> is quite different from the one in MgB<sub>2</sub>. In particular, while for MgB<sub>2</sub> the pairing is coming from the strong coupling between the  $\sigma$ -bands and the B-related  $E_{2g}$  phonon modes [16–19], in MoB<sub>2</sub> the pairing involves electronic states of the Mo- $d$  character and a combination of Mo-related low-frequency phonon modes with B-dominated ones [14, 20]. In fact, Quan *et al* [20] concluded that the source of the MoB<sub>2</sub>  $T_c$  is the so called electron-displaced atom scattering factor  $I^2$ , which is closely related to the electron-phonon (e-ph) matrix elements of the Eliashberg theory [21] (see equation 3). However, a detailed analysis about how this factor and other ingredients involved in conventional superconductivity (like phonon frequencies, linewidths, or electron-phonon coupling parameter) are evolving as a function of pressure is lacking.

In this paper we present a thorough study of the lattice dynamics, electron-phonon coupling, and superconducting  $T_c$  of  $\alpha$ -MoB<sub>2</sub> as a function of applied pressure, from 70 GPa to 300 GPa, within the framework of density functional theory (DFT) [22] and density functional perturbation theory (DFPT) [23–26] using a mixed-basis pseudopotential method [27]. Superconducting properties are analyzed in the framework of the Eliashberg theory [21]. We give a detailed description of the phonon linewidths and electron-phonon coupling as a function of applied pressure. In particular, we analyze the contributions of different phonon modes to these quantities, and determine its specific role for inducing the high  $T_c$  value of  $\alpha$ -MoB<sub>2</sub>. For comparison, we also present a similar analysis for the sibling system NbB<sub>2</sub>, which is a low- $T_c$  superconductor with intermediate coupling. The paper is organized as follows. In section 2 we describe the computational details of our calculations. The results for the evolution of lattice dynamics, e-ph coupling and  $T_c$  as a function of pressure are presented in section 3. Finally, in section 4 the main findings are summarized.

## 2. Computational details

The present density-functional calculations [22] were performed with the mixed-basis pseudopotential method (MBPP) [27]. Norm-conserving pseudopotentials for Mo, Nb, and B were generated according to the Vanderbilt description [28] and include partial-core correction. For Mo and Nb, semicore  $4s$  and  $4p$  states were taken into the valence space. The current method applies a mixed-basis scheme, which uses a combination of local functions and plane waves for the representation of the valence states. We used  $s$ ,  $p$ , and  $d$ -type functions for Mo and Nb, while for B only  $s$  and  $p$ -type, supplemented by plane waves up to a kinetic energy of 32 Ry. Present calculations were performed with the PBE [29] form of the GGA exchange-correlation functional. The Monkhorst-Pack special  $k$ -point sets technique, with a Gaussian smearing of 0.25 eV and a grid of  $18 \times 18 \times 18$ , was used for the Brillouin-zone integration. Phonon properties are calculated via density functional perturbation theory (DFPT) [23, 24] as implemented in the MBPP code [25, 26]. The phonon dispersions are obtained by a Fourier interpolation of dynamical matrices calculated on a  $6 \times 6 \times 6$   $q$ -point mesh. For the calculation of e-ph coupling matrix elements, a denser  $36 \times 36 \times 36$   $k$ -point mesh was necessary.

Through the knowledge of the phonon dispersion and e-ph matrix elements the Eliashberg function is accessible,

$$\alpha^2 F(\omega) = \frac{1}{2\pi\hbar N(E_F)} \sum_{\mathbf{q}\eta} \frac{\gamma_{\mathbf{q}\eta}}{\omega_{\mathbf{q}\eta}} \delta(\omega - \omega_{\mathbf{q}\eta}), \quad (1)$$

with  $N(E_F)$  as the electronic density of states at the Fermi level, per atom and spin;  $\omega_{\mathbf{q}\eta}$  as the frequency of the phonon mode at the  $\mathbf{q}$ -vector and branch  $\eta$ , and the phonon linewidths  $\gamma_{\mathbf{q}\eta}$  given by

$$\gamma_{\mathbf{q}\eta} = 2\pi\omega_{\mathbf{q}\eta} \sum_{\mathbf{k}\nu\nu'} |g_{\mathbf{k}+\mathbf{q}\nu',\mathbf{k}\nu}^{\mathbf{q}\eta}|^2 \delta(\epsilon_{\mathbf{k}\nu} - E_F) \delta(\epsilon_{\mathbf{k}+\mathbf{q}\nu'} - E_F), \quad (2)$$

where  $\epsilon_{\mathbf{k}\nu}$  is the one-electron band energy with momentum  $\mathbf{k}$  and band index  $\nu$ . In the last equation,  $g_{\mathbf{k}+\mathbf{q}\nu',\mathbf{k}\nu}^{\mathbf{q}\eta}$  represents the coupling matrix element for scattering of an electron from a  $\mathbf{k}\nu$  electronic state to another  $\mathbf{k} + \mathbf{q}\nu'$  state, by a phonon  $\mathbf{q}\eta$ , and is given by

$$g_{\mathbf{k}+\mathbf{q}\nu',\mathbf{k}\nu}^{\mathbf{q}\eta} = \sqrt{\frac{\hbar}{2\omega_{\mathbf{q}\eta}}} \sum_{\kappa a} \frac{1}{\sqrt{M_\kappa}} \eta_{\kappa a}^{\mathbf{q}\eta} \langle \mathbf{k} + \mathbf{q}\nu' | \delta_{\kappa a}^{\mathbf{q}} V | \mathbf{k}\nu \rangle, \quad (3)$$

with  $M_\kappa$  as the mass of the  $\kappa$ -th atom in the unit cell, and  $\eta_{\kappa a}^{\mathbf{q}\eta}$  as the normalized eigenvector of the corresponding phonon mode  $\mathbf{q}\eta$ . The quantity  $\delta_{\kappa a}^{\mathbf{q}} V$  represents the first-order change of the total crystal potential, with respect to the displacement of the  $\kappa$ -th atom in the  $a$  direction.

From  $\alpha^2 F(\omega)$  we can obtain some useful integrated quantities, like the average Allen-Dynes characteristic phonon frequency  $\omega_{\log}$

$$\omega_{\log} = \exp\left(\frac{2}{\lambda} \int_0^\infty d\omega \frac{\ln(\omega)}{\omega} \alpha^2 F(\omega)\right), \quad (4)$$

the square-average phonon frequency  $\bar{\omega}_2$

$$\bar{\omega}_2 = \langle \omega^2 \rangle^{1/2} = \left( \frac{2}{\lambda} \int_0^\infty d\omega \alpha^2 F(\omega) \omega \right)^{1/2}, \quad (5)$$

the average e-ph coupling constant  $\lambda$

$$\lambda = 2 \int_0^\infty \frac{d\omega}{\omega} \alpha^2 F(\omega) = \frac{1}{\pi \hbar N(E_F)} \sum_{\mathbf{q}\eta} \frac{\gamma_{\mathbf{q}\eta}}{\omega_{\mathbf{q}\eta}^2}, \quad (6)$$

as well as the frequency-dependent  $\lambda$ , given by:

$$\lambda(\omega) = 2 \int_0^\omega \frac{d\omega'}{\omega'} \alpha^2 F(\omega'). \quad (7)$$

Finally,  $\alpha^2 F(\omega)$  is used to determinate the superconducting critical temperature,  $T_c$ , by solving the Eliashberg gap equations [21, 30] numerically.

### 3. Results and discussion

The  $\alpha$ -MoB<sub>2</sub> has an AlB<sub>2</sub>-type structure, consisting of planar close packed layers of Mo (at (0, 0, 0), 1a Wyckoff position) and B atoms (at (2/3, 1/3, 1/2), 2d Wyckoff position) alternated along the  $c$ -axis of the hexagonal unit cell [14, 15, 31]. Its structure was fully optimized by energy minimization, that is, for each fixed  $V$  the  $c/a$  parameter was optimized in order to get the  $E(V)$  and  $p(V)$  equations of state (see figure 1).

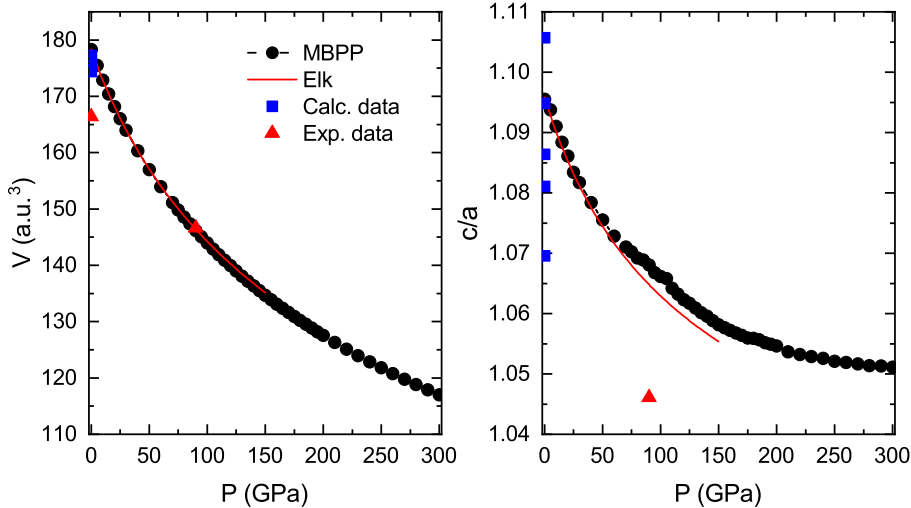


**Figure 1.** Calculated  $p(V)$  equation of state and optimized  $c/a$  parameter, as a function of applied pressure for  $\alpha$ -MoB<sub>2</sub> obtained by two different band-structure methods (MBPP [27] and Elk [32]), compared with experimental data [14, 31] (red triangles), and calculated results reported previously [33–37] (blue squares).

The current results are compared with available experimental data [14, 31], as well as reported calculated values [33–37]. Our results are in remarkable agreement with the

data of Pei *et al* [14, 31] at 90 GPa for both, the volume (a difference of around 0.3%) and also the  $c/a$  ratio (difference of 2.1%). In addition, structure-optimization calculations were also performed with the full-potential Elk code [32], showing an excellent agreement with the MBPP-code calculations, which demonstrates the high accuracy of the constructed pseudopotentials.

The comparison of the electronic band structure and density of states for two different pressure values, 70 GPa and 120 GPa, is presented in figure 2. As already pointed out previously [20], the bands around the Fermi level ( $E_F$ ) are dominated by the Mo  $d$  states, with a very minor participation of B states. This property is maintained across the whole pressure range, and results in very modest changes around the Fermi level. The main pressure effects are a band-width increase and a small reduction of the states at the Fermi level ( $N(E_F)$ ).

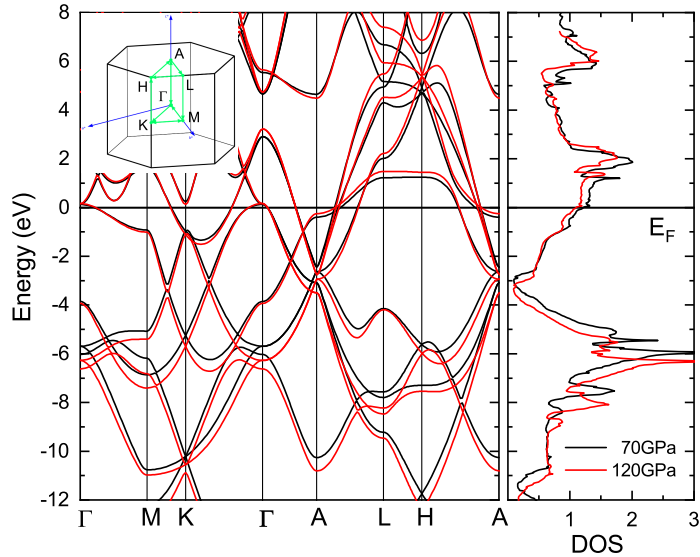


**Figure 2.** Comparison of the electronic band structure and density of states (DOS) for 70 GPa and 120 GPa. The first Brillouin zone for the hexagonal structure is presented as inset (generated by XCrySDen) [38].

In figure 3 the phonon dispersion along high-symmetry directions as well as its corresponding phonon density of states (PHDOS), for specific applied pressure values, are presented. The chosen pressures span across the stability region of the  $\alpha$ -MoB<sub>2</sub> structure [14]. The main characteristics of the phonon spectrum, as previously observed [14, 20], are found for the whole pressure range. On the one hand, the low-frequency region dominated by Mo vibrations; the high-frequency one ruled by B modes; and the frequency gap that separates them. On the other hand, the acoustic low-frequency modes along the L-A path, which exhibit a phonon anomaly close to L-point, as well as the soft acoustic branches along the A-H and H-L paths. Interestingly, the acoustic mode with lowest frequency (labeled as A3) is the one with the largest e-ph coupling constant contribution, given by the red vertical lines in figure 3. In general, the main effect of the applied pressure on the phonon spectra is a generalized hardening of the phonon frequencies, which directly weakens the observed phonon anomaly at the L-A path, and reduces at the same time its strong e-ph contribution.

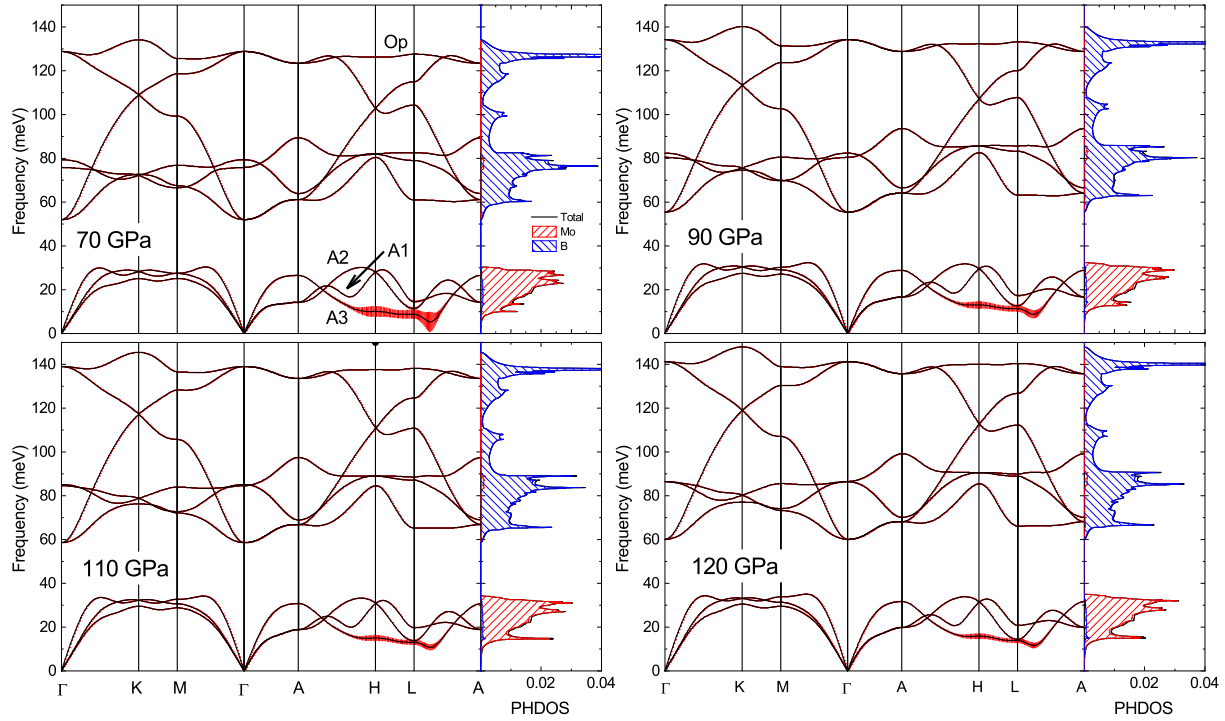


**Figure 3.** Phonon dispersions and phonon density of states (PHDOS) for  $\alpha$ -MoB<sub>2</sub>, calculated at selected pressures: 70 GPa, 90 GPa, 110 GPa, and 120 GPa. Vertical red lines correspond to the e-ph coupling constant  $\lambda_{q\eta}$ . The labels correspond to the acoustic phonon branches (A1, A2, and A3), as well as the highest-optic one (Op) at the A–H–L–A paths.

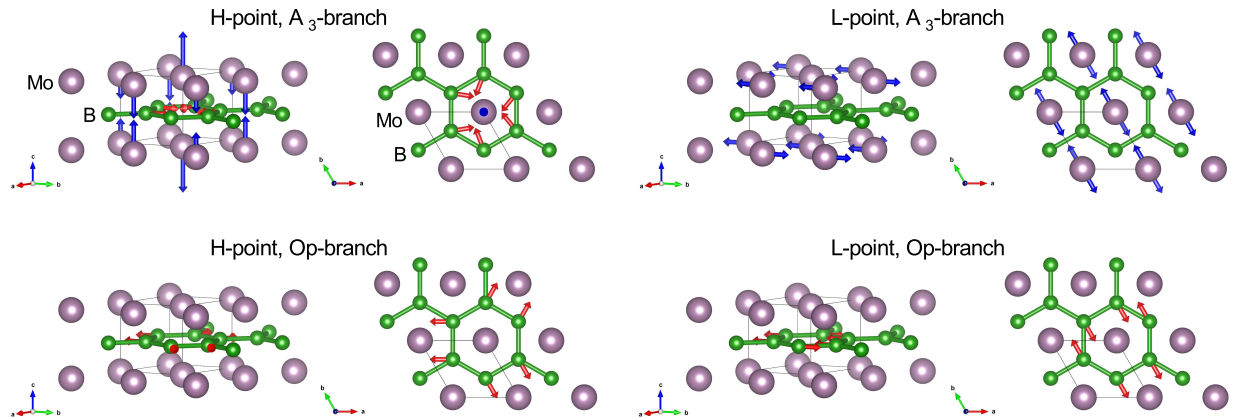


**Figure 4.** Phonon modes corresponding to the acoustical A3 and optical Op branches at the H- and L-points [39]. The size of the arrows indicate the vibrational directions and the corresponding magnitude. For the case of the H-point A3-branch, the B related arrows were scaled (4X) in order to be noticeable.

In addition, we also present the phonon modes corresponding to the acoustical A3 and optical Op branches at the H- and L-points of the IBZ (figure 4). The displacement patterns show that the A3 related modes are clearly dominated by Mo atoms, while the Op ones are ruled completely by the B atoms.

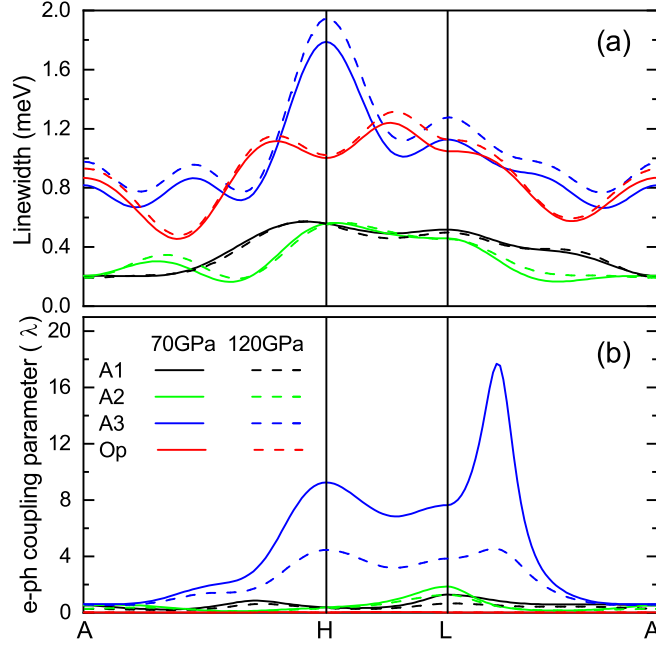


**Figure 5.** (a) Linewidths and (b) e-ph coupling constant for  $\alpha$ -MoB<sub>2</sub>, at 70 GPa (solid lines) and 120 GPa (dashed lines) along the A–H–L–A paths, for the three acoustic branches (A1, A2, and A3) and the highest-frequency optical branch (Op).

A closer inspection of the individual phonon linewidths and mode couplings revealed that important contributions are attributed to the acoustic phonon branches (A1, A2, and A3) and the highest optic one (Op), in particular along at the A–H–L–A paths (figure 3). In figure 5, linewidths and e-ph coupling constants of these modes are shown along these high-symmetry directions for two pressures. The largest linewidths (figure 5a) are found for the A3 branch, with a particular strong peak located at the H-point, followed closely by the Op branch. These results indicate an important participation of phonon modes dominated by Mo (A3) and also by B (Op) in the e-ph coupling (equation 2) reflected by the phonon linewidths (equation 3). However, for the e-ph coupling constants shown in figure 5b, the influence of B phonon-modes is faded away due to the factor  $1/\omega_{\mathbf{q}\eta}^2$  entering its definition (equation 6). In contrast, the large e-ph coupling constants of the acoustic branch A3 is boosted by the low frequencies of these Mo phonon modes, especially around the phonon anomaly close to the L-point. With increasing pressure, while the linewidths increase a little bit,  $\lambda_{\mathbf{q}\eta}$  strongly reduces, correlating with the observed hardening of this acoustic branch.

In order to analyze the evolution of the superconducting properties as a function of pressure, the Eliashberg function  $\alpha^2F(\omega)$ , the e-ph coupling constant  $\lambda$ , the Allen-Dynes

characteristic phonon frequency  $\omega_{log}$ , and the square-average phonon frequency  $\bar{\omega}_2$  were calculated for each case.

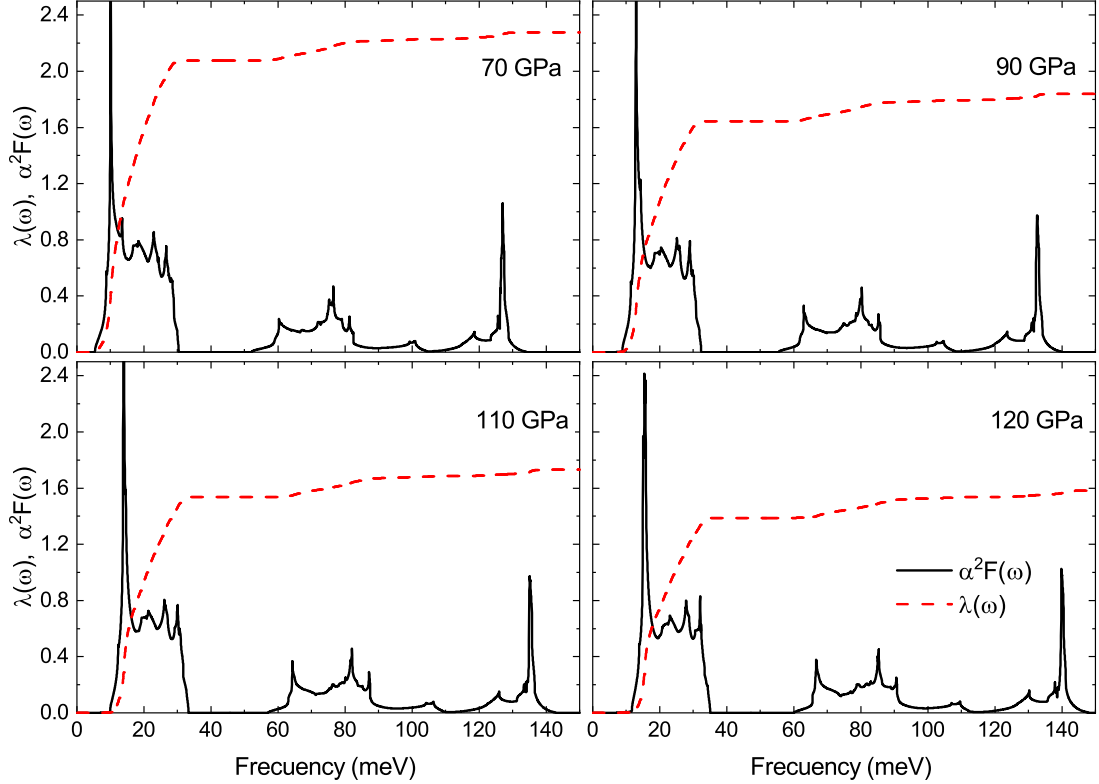


**Figure 6.**  $\alpha$ -MoB<sub>2</sub> Eliashberg function  $\alpha^2F(\omega)$  (black solid line) and frequency-dependent e-ph coupling constant  $\lambda(\omega)$  (red dashed line) for specific applied pressure values.

The Eliashberg functions for selected pressures are presented in figure 6, together with  $\lambda(\omega)$ . In all cases, the largest contribution for  $\alpha^2F(\omega)$  and  $\lambda(\omega)$  comes from the acoustic low-frequency region, dominated almost completely by Mo phonon modes along the A-H, H-L, and specially the L-A paths, where the phonon anomaly is located. As expected, the largest coupling corresponds to the pressure that is closest to the phase transition: 70 GPa with  $\lambda \approx 2.3$ . As pressure increases, the coupling reduces, at the same time that the observed phonon anomaly attenuates, which is a direct consequence of the general hardening of the phonon spectrum, as previously discussed.

The evolution of the coupling related quantities, namely the density of states at the Fermi level ( $N(E_F)$ ),  $\omega_{log}$ ,  $\bar{\omega}_2$ , and  $\lambda$ , as a function of pressure, are presented in figure 7. There is a nice agreement of these quantities with the reported values in literature at 90 GPa [14, 20], although our calculated  $\lambda = 1.84$  is slightly larger (between 10% and 15%). This can be due to the slight difference on the structural parameters (see figure 1) or pseudopotential construction. From the evolution of  $\lambda$ , it can be seen that the strong pressure dependence of the coupling is coming mainly from the low-frequency phonons (traced by  $\omega_{log}$  and  $\bar{\omega}_2$ ),



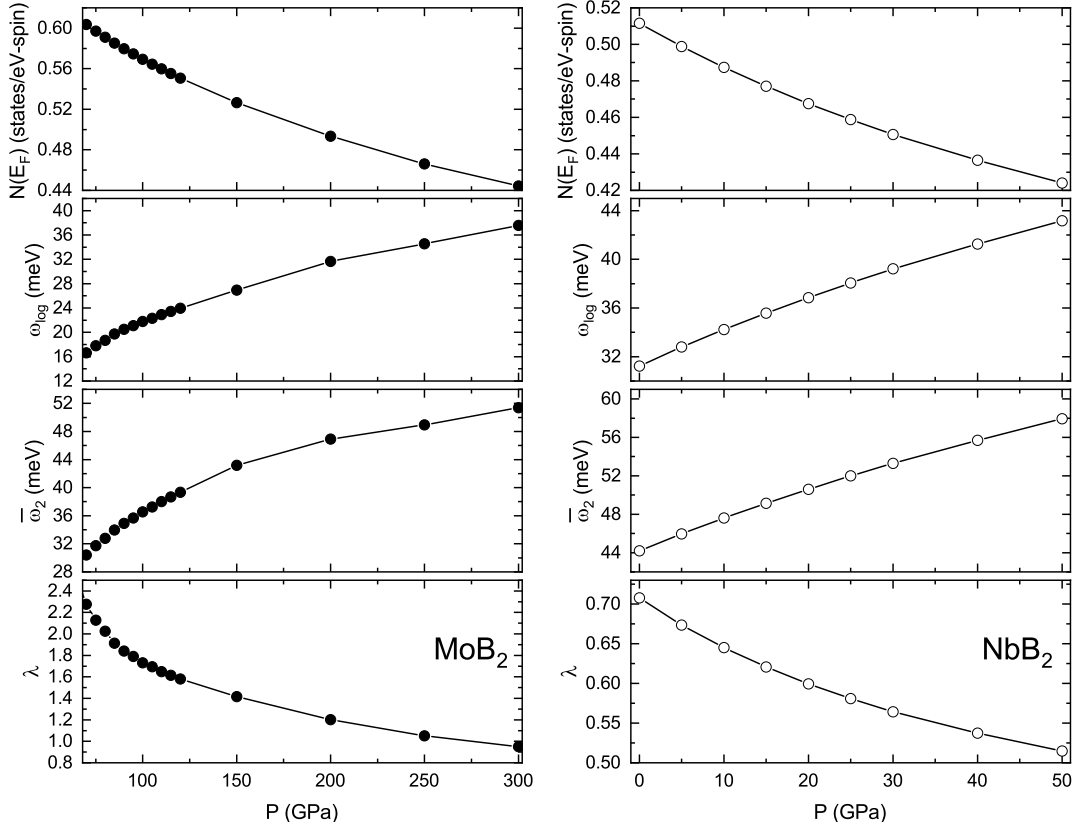


**Figure 7.** Density of states at the Fermi level ( $N(E_F)$ ), the Allen-Dynes characteristic phonon frequency ( $\omega_{log}$ ), the square-average phonon frequency ( $\bar{\omega}_2$ ), and the e-ph coupling constant ( $\lambda$ ), as a function of applied pressure, for  $\alpha$ -MoB<sub>2</sub> (left) and NbB<sub>2</sub> (right).

while  $N(E_f)$  does not exhibit dramatic changes as a function of pressure.  $\alpha$ -MoB<sub>2</sub> remains in the strong-coupling regime until 300 GPa, where  $\lambda = 0.95$ , while  $\omega_{log} = 37.58$  meV, and  $\bar{\omega}_2 = 51.39$  meV.

For comparison, we also calculated the same e-ph parameters, as a function of applied pressure, for the sibling compound NbB<sub>2</sub> (with the same crystal structure) at its own optimized structural parameters (see figure 7). NbB<sub>2</sub> was studied more or less at the same time when superconductivity in MgB<sub>2</sub> was discovered. This was done with the idea to find related materials with improved superconducting properties. It turned out, however, that NbB<sub>2</sub> has an intermediate coupling ( $\lambda = 0.67$ ) and a low  $T_c$  value (approx. 8.4 K) [40]. Although NbB<sub>2</sub> has lower  $\lambda$  values than MoB<sub>2</sub> (the highest calculated  $\lambda$  for NbB<sub>2</sub> is 0.71 at  $p = 0$  GPa), the trends as a function of pressure for the coupling-related quantities are basically the same: a reduction of  $N(E_F)$ , a phonon hardening, and a  $\lambda$  decrease.

In order to analyze the evolution of  $T_c$  as a function of pressure, we applied three different schemes: (1), the standard Allen-Dynes equation [41],

$$T_c^{AD} = \frac{\omega_{log}}{1.20} \exp\left(-\frac{1.04(1+\lambda)}{\lambda - \mu^*(1+0.62\lambda)}\right), \quad (8)$$

(2), the corrected Allen-Dynes equation for strong-coupling systems (normally for  $\lambda \leq 1.3$ )

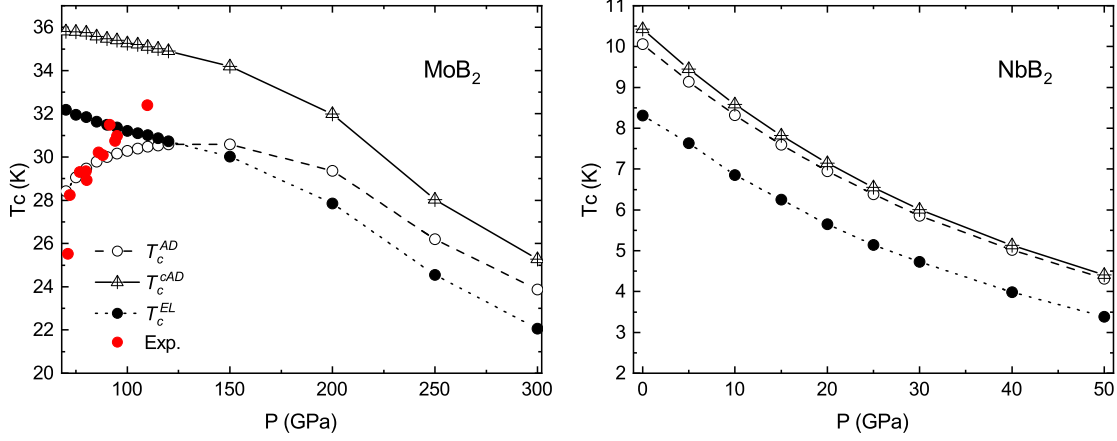


**Figure 8.** Evolution of  $T_c$  as a function of pressure for  $\alpha$ -MoB<sub>2</sub> (left) and NbB<sub>2</sub> (right) using the standard Allen-Dynes [41] equation ( $T_c^{AD}$ ), the corrected Allen-Dynes equation ( $T_c^{cAD}$ ) [41], and the numerical solution of the isotropic Eliashberg gap equations ( $T_c^{EL}$ ) [21, 30]. Comparison with experimental results available in literature for  $\alpha$ -MoB<sub>2</sub> [14] (red dots).

[41],

$$T_c^{cAD} = \frac{f_1 f_2 \omega_{log}}{1.20} \exp\left(-\frac{1.04(1 + \lambda)}{\lambda - \mu^*(1 + 0.62\lambda)}\right), \quad (9)$$

where the correction factors to describe the strong-coupling regime are

$$f_1 = [1 + (\lambda/\Delta_1)^{3/2}]^{1/3}, \quad (10)$$

$$f_2 = 1 + \frac{(\bar{\omega}_2/\omega_{log} - 1)\lambda^2}{\lambda^2 + \Delta_2^2}, \quad (11)$$

and the parameters  $\Delta_1$  and  $\Delta_2$  given by

$$\Delta_1 = 2.46(1 + 3.8\mu^*), \quad (12)$$

$$\Delta_2 = 1.82(1 + 6.3\mu^*)(\bar{\omega}_2/\omega_{log}), \quad (13)$$

and finally (3), by solving the isotropic Eliashberg gap equations [21, 30] numerically,  $T_c^{EL}$ , using the calculated  $\alpha^2 F(\omega)$  for each considered pressure.

Results obtained for the three schemes, for both  $\alpha$ -MoB<sub>2</sub> and NbB<sub>2</sub>, are presented in figure 8, using in all cases the same Coulomb pseudopotential parameter  $\mu^* = 0.13$ , in order to be as close as possible to the previously reported  $T_c$  values for  $p = 90$  GPa [14, 20]. As expected, there are quantitative differences between the  $T_c$  estimates, in particular for the low-pressure region, where  $\alpha$ -MoB<sub>2</sub> is in the strong-coupling regime. While both strong-coupling schemes ( $T_c^{cAD}$  and  $T_c^{EL}$ ) predict a monotonous superconducting temperature reduction as a function of pressure,  $T_c^{AD}$  first increases slightly from 70 GPa to approximately 150 GPa,

followed by a decrease. For  $p > 250$  GPa,  $T_c^{AD}$  and  $T_c^{cAD}$  are getting closer, a clear indication of the transition to a more moderate coupling region. For NbB<sub>2</sub>, all three  $T_c$  estimates reveal the same pressure dependence, while  $T_c^{AD}$  and  $T_c^{cAD}$  agree almost quantitatively. This behavior is expected, since NbB<sub>2</sub> has an e-ph coupling that goes from intermediate to low coupling strength, as applied pressure increases. From these results it is clear that the use of  $T_c^{AD}$  is not adequate for a strong-coupling system like  $\alpha$ -MoB<sub>2</sub>, showing misleading values and even wrong tendencies, as noted previously [20]. A possible reason of the apparent disagreement between our calculated  $T_c$  with experimental data [14] is that, very likely, the measured MoB<sub>2</sub> samples below  $p = 90$  GPa possess a different crystal structure, or consist of a mix of different phases, as mentioned by the authors of the experimental work. However, for pressures at (or above) 90 GPa, our calculated  $T_c^{EL}$  (by solving the Eliashberg gap equations) are around  $\pm 1$  K from the reported measurements and, interestingly,  $T_c^{EL}$  shows the best agreement with the reported experimental data at 90 GPa. We note that, within the framework of the Eliashberg theory, solving the (isotropic) gap equations with  $\alpha^2F(\omega)$  as input is the most direct way to calculate the superconducting temperature, and is superior to the other two approaches, which only provide approximations to its solution. Such a  $T_c$  reduction as a function of applied pressure, as obtained from our calculations for  $\alpha$ -MoB<sub>2</sub> and NbB<sub>2</sub>, is also observed experimentally for Nb-substituted MoB<sub>2</sub> (Nb<sub>0.25</sub>Mo<sub>0.75</sub>B<sub>2</sub>) [42]. There, a steady  $T_c$  reduction is reported from 8 K at 0 GPa to 4 K at 50 GPa, followed by a gradual rise to 5.5 K at 170 GPa that is accompanied by a significant broadening of the superconducting transition width [42].

#### 4. Conclusions

To summarize, we have performed a first-principles linear-response study of the lattice dynamical properties, electron-phonon coupling, and superconductivity of  $\alpha$ -MoB<sub>2</sub> as a function of applied pressure (from 70 GPa to 300 GPa). We found that the electron-phonon interaction induces large phonon linewidths for modes located specifically along the A–H, H–L, and L–A high-symmetry paths, where a phonon anomaly is present. The largest linewidths are displayed by the highest-frequency optical phonon mode (ruled by B vibrations) and the acoustic low-frequency phonon modes (involving mainly Mo atoms). However, the contribution of the optical phonon mode to the electron-phonon coupling constant is diminished because of its high-frequency value, while the dominating one is coming from the lowest-frequency acoustic phonon mode. As pressure increases, the phonon spectrum hardens, in particular the acoustic low-frequency phonon modes, and the electron-phonon coupling constant decreases, while the density of states at the Fermi level barely changes. Estimates for  $T_c$ , obtained either way by the corrected Allen-Dynes equation or by solving the Eliashberg gap equations, show a decrease as a function of applied pressure, which correlates with the phonon hardening and the reduction of  $\lambda$ . We found a good agreement between the experimental  $T_c$  values and the calculated ones for 90 GPa and 110 GPa. However, data for larger applied pressure values are needed to allow a more complete assessment of the predicted tendencies of  $T_c$  for  $\alpha$ -MoB<sub>2</sub>.

## Acknowledgments

This research was partially supported by the Consejo Nacional de Humanidades, Ciencias y Tecnologías (CONAHCYT, México) under Grant No. FOP16-2021-01-320399; Vicerrectoría de Investigación (VIEP), Benemérita Universidad Autónoma de Puebla (BUAP) under Grant No. 100517450-VIEP2023; and the Karlsruher Institut für Technologie (KIT), Germany.

## References

- [1] Nagamatsu J, Nakagawa N, Muranaka T, Zenitani Y and Akimitsu J 2001 *Nature* **410** 63
- [2] Buzea C and Yamashita T 2001 *Supercond. Sci. Technol.* **14** R–115
- [3] Kazakov S M, Karpinski J, Jun J, Geiser P, Zhigadlo N D, Puzniak R and Mironov A V 2004 *Physica C* **408-410** 123
- [4] Karpinski J, Zhigadlo N D, Schuck G, Kazakov S M, Batlogg B, Rogacki K, Puzniak R, Jun J, Müller E, Wägli P, Gonelli R S, Daghero D, Umrinario G A and Stepanov V A 2005 *Phys. Rev. B* **71** 174506
- [5] Daghero D, Delaude D, Calzolari A, Tortello M, Umarino G U, Gonnelli R S, Stepanov V A, Zhigadlo N D, Katrych S and Karpinski J 2008 *J. Phys.: Condens. Matter* **20** 085225
- [6] la Peña Seaman O D, de Coss R, Heid R and Bohnen K P 2010 *Phys. Rev. B* **82** 224508
- [7] Monteverde M, nez Regueiro M N, Rogado N, Regan K A, Hayward M A, He T, Loureiro S M and Cava R J 2001 *Science* **292** 75
- [8] Wang Y, Lv J, Ma Y, Cui T and Zou G 2009 *Phys. Rev. B* **80** 092505
- [9] Renker B, Bohnen K P, Heid R, Ernst D, Shober H, Koza M, Adelman P, Schweiss P and Wolf T 2002 *Phys. Rev. Lett.* **88** 067001
- [10] Leyarovska L and Leyarovski E 1979 *J. Less-Common Met.* **67** 249
- [11] Kotegawa H, Ishida K, Kitaoka Y, Muranaka T, Nakagawa N, Takagiwa H and Akimitsu J 2002 *Physica C* **378-381** 25
- [12] Takeya H, Togano K, Sung Y S, Mochiku T and Hirata K 2004 *Physica C* **408-410** 144
- [13] Muzzy L E, Avdeev M, Lawes G, Haas M K, Zandbergen H W, Ramirez A P, Jorgensen J D and Cava R J 2002 *Physica C* **382** 153
- [14] Pei C, Zhang J, Wang Q, Zhao Y, Gao L, Goung C, Tian S, Luo R, Li M, Yang W, Lu Z Y, Lei H, Liu K and Qi Y 2023 *Natl. Sci Rev.* **nwad034**
- [15] Jones M and Marsh R 1954 *J. Am. Chem. Soc.* **76** 1434
- [16] Kortus J, Mazin I I, Belashchenko K D, Antropov V P and Boyer L L 2001 *Phys. Rev. Lett.* **86** 4656
- [17] Floris A, Sanna A, Lüders M, Profeta G, Lathiotakis N N, Marques M A L, Franchini C, Gross E K U, Continenza A and Massidda S 2007 *Physica C* **456** 45
- [18] Bohnen K P, Heid R and Renker B 2001 *Phys. Rev. Lett.* **86** 5771
- [19] Geerk J, Schneider R, Linker G, Zaitsev A G, Heid R, Bohnen K P and v Löhneysen H 2005 *Phys. Rev. Lett.* **94** 227005
- [20] Quan Y, Lee K W and Pickett W E 2021 *Phys. Rev. B* **104** 224504
- [21] Eliashberg G M 1960 *Sov. Phys. JETP* **11** 696
- [22] Kohn J W and Sham L J 1965 *Phys. Rev.* **140** A1133
- [23] Louie S G, Ho K M and Cohen M L 1979 *Phys. Rev. B* **19** 1774
- [24] Baroni S, de Gironcoli S and Corso A D 2001 *Rev. Mod. Phys.* **73** 515
- [25] Heid R, Bohnen K P and Ho K M 1998 *Phys. Rev. B* **57** 7407
- [26] Heid R and Bohnen K P 1999 *Phys. Rev. B* **60** R3709
- [27] Meyer B, Elsässer C, Lechermann F and Fähnle M FORTRAN90 Program for Mixed-Basis Pseudopotential Calculations for Crystals, Max-Planck-Institut für Metallforschung, Stuttgart (unpublished)
- [28] Vanderbilt D 1985 *Phys. Rev. B* **32** 8412
- [29] Perdew J P, Burke K and Ernzerhof M 1996 *Phys. Rev. Lett.* **77** 3865
- [30] Marsiglio F and Carbotte J 2003 **I. Conventional and High- $T_c$  Superconductors** pp 231

- [31] Tao Q, Zhao X, Chen Y, Li J, Li Q, Ma Y, Li J, Cui T, Zhu P and Wang X 2013 *RSC Advances* **3** 18317
- [32] The Elk Code <http://elk.sourceforge.net/>
- [33] Qi C, Jiang Y, Liu Y and Zhou R 2014 *Ceram. Int.* **40** 5843
- [34] Ding L P, Shao P, Zhang F H, Lu C, Ding L, Ning S Y and Huang X F 2016 *Inorg. Chem.* **55** 7033
- [35] Xu X, Fu K, Yu M, Lu Z, Zhang X, Liu G and Tang C 2014 *J. Alloy Compd.* **607** 198
- [36] Shein I R and Ivanovskii L 2006 *Phys. Rev. B* **73** 144108
- [37] Deligoz E, Colakoglu K and Ciftci Y O 2010 *Phys. Rev. B* **150** 405
- [38] Kokalj A 1999 *J. Mol. Graphics Modelling* **17** 176
- [39] Momma K and Izumi F 2011 *J. Appl. Crystallogr.* **44** 1272
- [40] Heid R, Renker B, Shober H, Adelman P, Ernst D and Bohnen K P 2003 *Phys. Rev. B* **67** 180510(R)
- [41] Allen P B and Dynes R C 1975 *Phys. Rev. B* **12** 905
- [42] Lim J, Sinha S, Hire A C, Kim J S, Dee P M, Kumar R S, Popov D, Hemley R J, Hennig R G, Hirschfeld P J, Stewart G R and Hamlin J J 2023